Theoretical Analysis of the Intermolecular Interaction Effects on the Excitation Energy of Organic Pigments: Solid State Quinacridone

Hiroo Fukunaga,*,† Dmitri G. Fedorov,‡ Mahito Chiba,‡ Kazumi Nii,§ and Kazuo Kitaura‡,||

Imaging Technology Center, Research & Development Management Headquarters, FUJIFILM Corporation, FFTP M0-6F, 1250, Takematsu, Minamiashigara-shi, Kanagawa 250-0111, Japan, Research Institute for Computational Sciences, National Institute of Advanced Industrial Science and Technology (AIST), 1-1-1 Umezono, Tsukuba, Ibaraki 305-8568, Japan, Synthetic Organic Chemistry Laboratories, Research & Development Management Headquarters, FUJIFILM Corporation, 577, Ushijima, Kaisei-machi, Ashigarakami-gun, Kanagawa 258-8577, Japan, and Graduate School of Pharmaceutical Sciences, Kyoto University, Sakyo-ku. Kyoto 606-8501, Japan

Received: June 4, 2008; Revised Manuscript Received: August 12, 2008

Quinacridones (QAs) are organic hydrogen-bonded pigments, which are yellow in solution and become reddish to violet in solid phase depending on the crystal structure. We have carried out regular and fragment molecular orbital (FMO) based time-dependent density functional theory (TDDFT) calculations of the α^{I}, β, and γ crystalline phases of QA to examine the origin of the spectral shift in the solid phase. On the basis of the TDDFT calculations, we have found that the spectral shift from gas to solid phase in QA is dominated by the interplay of the structural deformation, electrostatic potential (crystal field), and intermolecular interactions, and each contribution is of the same order of magnitude. The spectral shift induced by the structural deformation is mainly caused by the stretch of the C═O bond. The individual intermolecular interactions contribute to bathochromic and hypsochromic shifts depending on the spatial orientation, and their sums result in the bathochromic shift overall.

I. Introduction

In general, the organic pigment has a stronger resistance to light, heat, and chemicals than the colorant. The stability of the pigment is due to the intermolecular interactions in the crystalline phases. In addition, most organic pigments exhibit different colors in solid state from those in solution. The spectral shift from solution to solid state also strongly depends on the intermolecular interactions such as hydrogen bonds (HB) and van der Waals (vdW) forces determined by the crystal packing. Thus, the intermolecular interactions strongly influence the chemical, physical and optical properties of pigments. To examine the effect of the intermolecular interactions on the electronic structures of the hydrogen-bonded pigments, we chose the linear *trans*-quinacridone (QA) as a typical example and carried out time-dependent density functional theory (TDDFT) calculations for excitations in the solid state.

QAs are industrially important organic pigments, for which there have been extensive studies of the crystal structures,[1−6] the absorption spectra in solution as well as in solid state,[7−10] and the effect of intermolecular interactions in the crystalline phase on the absorption spectra.[11−15] Though there are a few theoretical analyses of QA based on the quantum-chemical calculations,[16,17] they are not sufficient for understanding the absorption spectra in solid state.

The crystal structures of QA have been reported for the four polymorphs of the α^{I}-,[5] α^{II}-,[2] β-,[4,5] and γ-phases.[1,3,5] These crystal structures are mainly characterized by the NH···O intermolecular hydrogen bonds. Both in the α^{I} and β crystalline phases, each molecule is connected by hydrogen bonds to two neighboring molecules and a molecular chain is formed, but the alignment of the hydrogen bonding chains is different from each other; i.e., all chains are parallel in the α^{I}-phase, while there are two different chain arrangements in the β-phase. In the γ crystalline phase, each molecule is connected by a hydrogen bond to each of the four neighboring molecules, leading to a criss-cross pattern formation. The crystal structure of the α^{II} crystalline phase is controversial.[5,6] Therefore in this paper, we treat three crystalline phases: α^{I}, β, and γ.

The solution spectra of QA in dimethyl sulfoxide (DMSO) have been measured.[7,11,14] The absorption spectra accompanying a progression were assigned to the vibronic transition consisting of 0−0, 0−1, and 0−2 bands based on one electronic transition.[14] QAs, which are yellow in solution, become reddish to violet in solid phase. Mizuguchi et al. have reported that the spectral shift is interpreted as being due to the resonance interactions between transition dipoles aligned in the head-to-tail configuration using the exciton coupling model, and the intermolecular hydrogen bonds play an important role in the alignment of transition dipoles.[13,14] They have applied the interpretation to the other pigments such as diketopyrrolopyrrole[18] and perylene,[19] and the results were also in qualitative agreement with experiment.

The time-dependent density functional theory (TDDFT) method[20−25] has been widely used for the theoretical studies of photochemical processes. TDDFT calculations require much lower computational cost in comparison with high-level ab initio molecular orbital (MO) methods such as symmetry-adapted cluster configuration interaction (SAC-CI).[26,27] They are usually carried out with the Davidson-like subspace algorithm,[22] in which the computational cost is on the order of $O(N^3)$, where

* To whom correspondence should be addressed. Telephone: +81-465-85-2020. Fax: +81-465-85-2085. E-mail: hiroo_fukunaga@fujifilm.co.jp.
† Imaging Technology Center, FUJIFILM Corp.
‡ AIST.
§ Synthetic Organic Chemistry Laboratories, FUJIFILM Corp.
|| Kyoto University.

10.1021/jp804943m CCC: $40.75
Published on Web 10/04/2008

TABLE 1: Experimental Crystal Data for α^I-, β-, and γ-Quinacridones (Cell Parameters $a-c$ and Angles α, β, and γ; Cell Volume V; and the Number of Molecules per Unit Cell Z)

	crystalline phase		
	α^I	β	γ
space group	$P\bar{1}$	$P2_1/c$	$P2_1/c$
a/Å	3.802	5.692	13.70
b/Å	6.612	3.975	3.84
c/Å	14.485	30.02	13.35
α/deg	100.68	90	90
β/deg	94.40	96.76	100.09
γ/deg	102.11	90	90
V/Å^3	346.7	674.5	691.5
Z	1	2	2
ref.	5	5	3

N is the size of the system. Therefore, it is difficult to apply TDDFT for large molecular systems.

To reduce the computational cost for large systems, the fragment molecular orbital (FMO) method was originally proposed by Kitaura et al.[28] In the FMO method, the whole system is divided into fragments. The total energy in FMO is given by the sum of the fragment energies, fragment pair,[29] and, optionally, triple[30] contributions, which add explicit many-body corrections. The FMO method was combined with the electron correlation theories such as DFT,[31] second-order Møller−Plesset perturbation theory (MP2),[32] multiconfiguration self-consistent field (MCSCF),[33] and coupled cluster.[34] Excited-state calculations can be performed with FMO-based MCSCF,[33] configuration interaction method,[35,36] or TDDFT.[37,38] In this work we used the two-body expansion of FMO-TDDFT.[38] More details on fragmentation and the theory of FMO can be found in ref 39, and the recent review[40] has an overview of applications as well as theory development.

We carried out TDDFT calculations with cluster models based on the crystal structures and analyzed the effects of (1) the structural deformation by the crystal packing, (2) the crystal field (electrostatic potential), and (3) intermolecular interactions, on the spectral shifts. In addition, using FMO-TDDFT calculations based on the two-body expansion approximation, we examined the effect of individual intermolecular interactions on the spectral shift in detail.

II. Calculation Procedure

A. Molecular Structure Generation. We employed two kinds of structures for the excited-state calculations of QA. One is the optimized structure obtained at the restricted Hartree−Fock (RHF) level and the 6-31G(d,p) basis set,[41] which is used as a reference structure for the structural deformation by the crystal packing. The others are extracted from the X-ray crystal structures. In general, H atom positions cannot be exactly determined by the X-ray crystal structure analysis and to obtain the molecular structures in the α^I, β, and γ crystalline phases, we conducted partial geometry optimization, in which only the geometrical parameters related to H atoms are optimized while freezing the other geometrical parameters. Using the partial-optimized geometries, we regenerated the crystal structures accompanied with H atoms on the basis of the crystallographic data given in Table 1 as well as the fractional coordinates.[3,5]

B. Excited-State Calculations

For the excited-state calculations in the crystalline phases of QA, we employed cluster models based on the crystal structures,

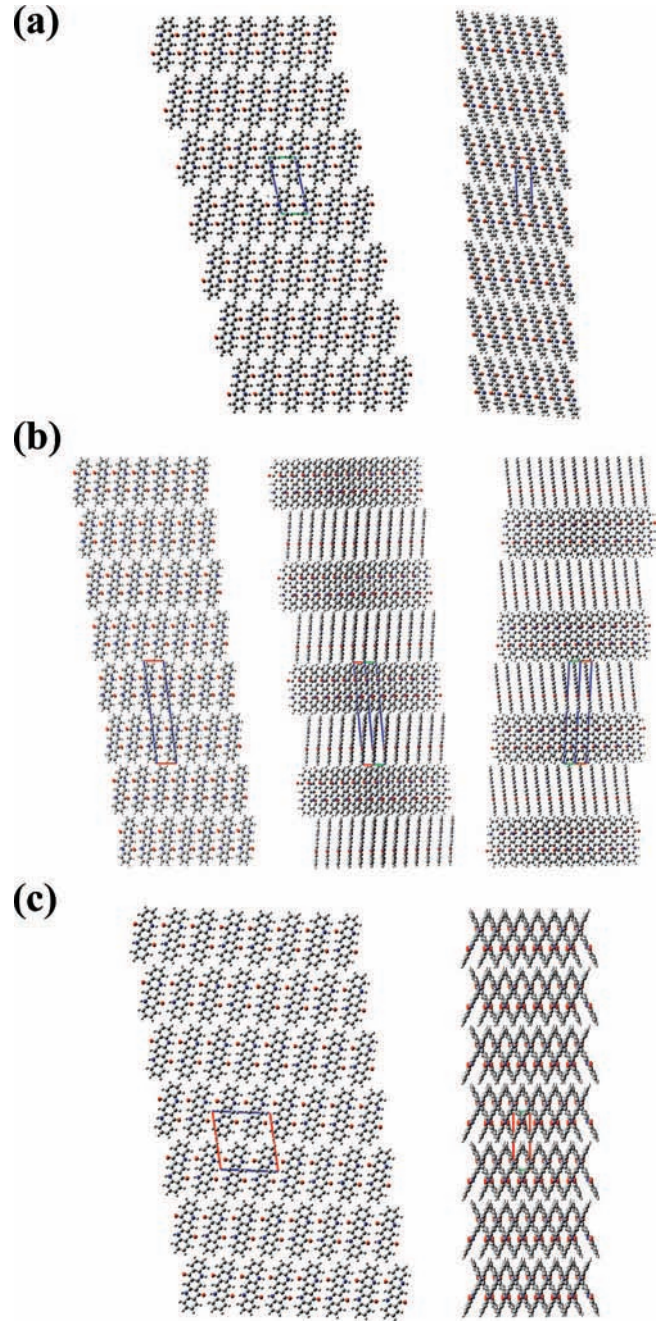

Figure 1. Cluster models from the crystal structures for the (a) α^I-, (b) β-, and (c) γ-phases used in TDDFT calculations. The red and blue spheres denote the O and N atoms, respectively, and the red, green, and blue lines forming trapezoids show the a-, b-, and c-axes of the unit cell, respectively. For each cluster, several views are depicted.

as shown in Figure 1. The α^I-cluster model is generated by repeating the unit cell 7, 7, and 7 times along the a-, b-, and c-axes, respectively, and the total number of molecules is 343, while in the β- and γ-cluster models each of which contain 392 molecules, with the unit cell repeated 7, 7, and 4 times along the a-, b-, and c-axes, respectively. Since we cannot directly treat the whole clusters in TDDFT calculations, we divided the constituent molecules into two groups: one (target group) is used for the explicit excited-state calculations, and the other provides the crystal field.

For the target group, we used two kinds of models to examine the effects of structural deformation, crystal field, and intermolecular interactions on the excitation energies separately. The first consists of only one molecule (1-mol. model), and the other

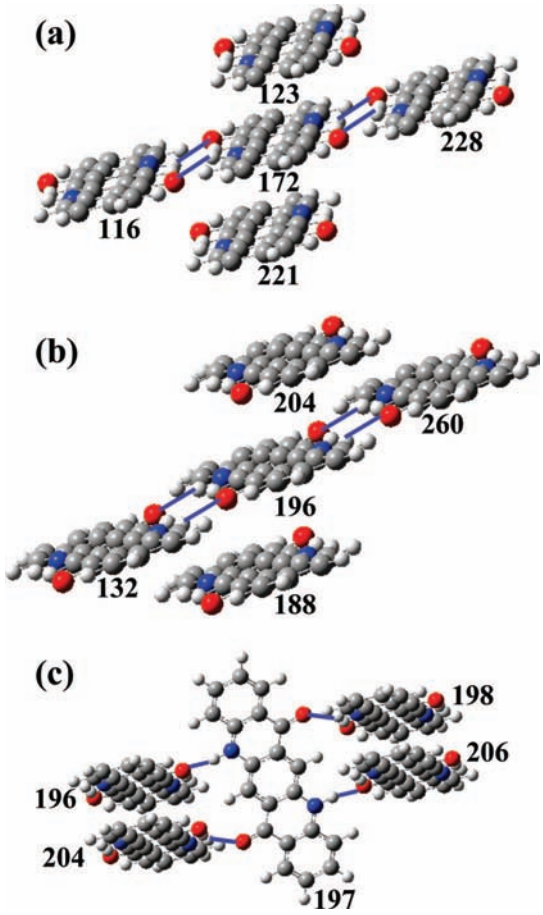

Figure 2. TDDFT 5-mol. models forming the central part of the larger clusters in Figure 1 for the (a) α^{I}-, (b) β-, and (c) γ-phases (other molecules in the larger clusters exerting the crystal field are not shown). The numbers represent the molecular ID referred to in the main text.

TABLE 2: Hydrogen Bond (HB) Distances (R), Angles ($\angle$), and Energies (E) for α^{I}-, β-, and γ-Quinacridones, from the B3LYP/6-31G(d,p) Calculations and the Experimental Structures

	HB pair		geom		
	ID1[a]	ID2[a]	R(NH···O)/Å	∠NH···O/deg.	E(HB)/(kcal/mol)
α^{I}	172	228	2.75	148	−12.4
β	196	260	2.89	163	−13.9
γ	197	198	2.76	164	−7.6

[a] IDs of molecules are shown in Figure 2.

has five molecules (5-mol. model) shown in Figure 2. In the 5-mol. models of the α^{I}- and β-phases, the central molecule interacts with the neighboring molecules via either hydrogen bond (formed with the 116th and 228th molecules for the α^{I}-phase, and 132th and 260th for the β-phase) or van der Waals (vdW) (123th and 221th for the α^{I}-phase, and 188th and 204th for the β-phase) interactions, while, for the γ-phase, the central molecule is connected by a hydrogen bond to each of the four neighboring molecules (196th, 198th, 204th, and 206th). The NH···O distances and the N−H···O angles in the crystal are given in Table 2. In addition, we evaluated the hydrogen bond energy in the ground state for each crystalline phase with RHF/6-31G(d,p), where a basis set superposition error correction is not included, and they are also indicated in Table 2. It is suggested from the geometrical and energetic points of view that the NH···O hydrogen bonds are strong for all of the crystalline phases.

The crystal field is approximated by the electrostatic potential (ESP) produced by the fractional point charges of atoms in the second group. The atomic charges were evaluated from Mulliken populations obtained from DFT calculations with the periodic boundary conditions (PBC), using the Becke's 1988 exchange functional[42] in conjunction with the LYP correlation functional[43] with the 6-31G(d,p) basis set (BLYP/6-31G(d,p)). The use of the BLYP functional is due to the present impossibility to use B3LYP with PBC.

The lowest vertical excitation energies and the corresponding oscillator strengths were calculated for the cluster models with TDDFT using the Becke's nonlocal three-parameter hybrid exchange functional (B3)[44] in conjunction with the LYP correlation functional with the 6-31G(d,p) basis set (B3LYP/6-31G(d,p)). In the calculations of excitation energies in solution, we employed the polarized continuum model (PCM).[45,46]

To analyze the excitation energy shifts caused by the individual intermolecular interactions in the crystal, we also conducted FMO-TDDFT calculations. In FMO-TDDFT, the excitation energy ΔE is calculated according to the following equation,

$$\Delta E = E^{*} - E^{\circ} = \Delta E_M + \sum_{I \neq M} \delta_{MI} \qquad (1)$$

where E^{*} and E° refer to the total energies of the excited state and the ground state, respectively. ΔE_{M} is the excitation energy of the central fragment. $\delta_{\mathrm{MI}} = \Delta E_{\mathrm{MI}} - \Delta E_{\mathrm{M}}$ are corrections to the excitation energy of M due to surrounding molecules I; ΔE_{MI} is the excitation energy of M + I molecular system. This quantity is used for the analysis of the excitation energy change due to the delocalization of M's orbital over I, including the charge transfer effect between M and I.

Here we denote the central molecule in the cluster models as M. TDDFT calculations are performed for M and all close pairs of M + I molecules involving M (for molecules I located up to about 5.2 Å from M); other molecules not included in TDDFT exert the crystal field (using PBC-derived atomic charges). This procedure differs from the conventional FMO-TDDFT because here we do not self-consistently polarize the fragment densities (we only perform the central fragment calculation once). The reason for this is the need to retain proper PBC charge distribution, eliminating the edge effects. Also, we used the point charge representation for all ESP in FMO.

In pairs of molecules the two nearly degenerate excitations from each molecule interact, resulting in a pair of split excitations (degenerating into the zone structures for infinite size). To compute the pair corrections δ_{MI}, one of the excitations should be selected, and we picked the one with the larger oscillator strength. Note that, in cluster models computed with the regular TDDFT, the same problem occurred on the level of five coupled excitations (since the clusters contain five molecules), and by plotting the orbitals it was established that the excitation with the largest oscillator strength is the desired one.

The number of explicit TDDFT pairs in FMO was 20, 14, and 18, for α^{I}-, β-, and γ-structures, respectively (corresponding to 504−720 atoms; another 11628−13608 atoms were treated as point charges). The excited state of interest was not always the lowest, and we calculated four excited states in FMO-TDDFT and 11 states at most in the regular TDDFT to capture the desired state. Throughout this work, we computed vertical excitation energies with the same geometry for the ground and excited states.

Geometry optimization as well as TDDFT calculations were performed using the Gaussian03 package[47] and FMO-TDDFT

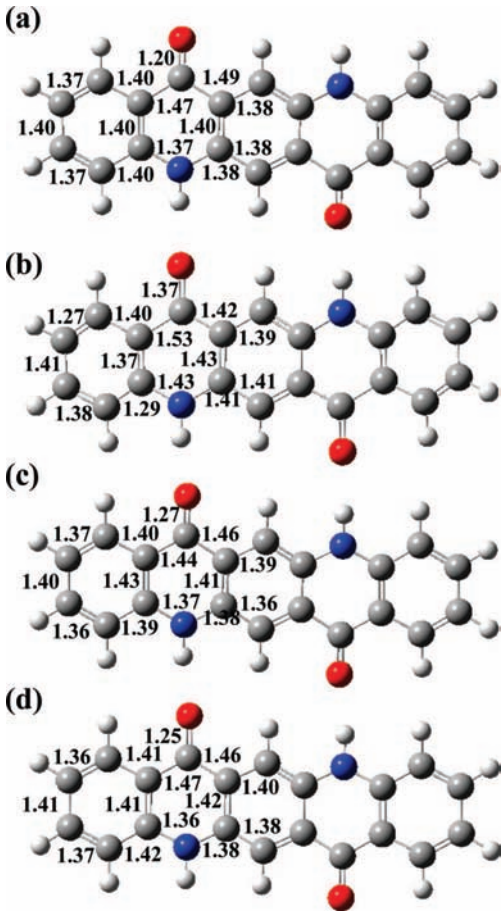

Figure 3. (a) RHF/6-31G(d,p) optimized geometry, and the geometries extracted from the experimental crystal structures for the (b) α^{I}-, (c) β-, and (d) γ-phases. The numerical values show bond lengths in angstroms.

TABLE 3: TDDFT/B3LYP/6-31G(d,p) Excitation Energies ΔE (eV) and Oscillator Strengths f Using One Molecule (1-mol.) and Five Molecules (5-mol.) Cluster Models with and without the Electrostatic Potential (ESP) Representing the Crystal Field

		1-mol. model				5-mol. model	
		without ESP		with ESP		with ESP	
phase	exptlΔE	ΔE	f	ΔE	f	ΔE	f
gas[a]		2.88	0.07				
solution[b]	2.37	2.70 [a]	0.10				
crystal α^{I}	2.22[c]	2.51	0.07	2.37	0.07	2.22	0.17
crystal β	2.17[c], 2.14[d]	2.75	0.07	2.65	0.07	2.47	0.16
crystal γ	2.25[d], 2.17[e]	2.78	0.07	2.66	0.06	2.49	0.22

[a] Gas phase RHF/6-31G(d,p) optimized geometry. [b] In DMSO, experiment ref 14, calculations with PCM in this work. [c] Reference. 8. [d] Reference. 10. [e] Reference. 14.

calculations using the GAMESS package.[48] The standard parameters were used to set up the accuracy in all calculations.

III. Results

A. Absorption Spectra in Solution. To assign the absorption spectrum of QA, we performed TDDFT calculations in the gas phase and in DMSO with the RHF-optimized geometry shown in Figure 3a. Table 3 indicates the calculated excitation energies and oscillator strengths as well as the observed values. The vertical excitation energy, which is estimated at 2.88 eV in the gas phase, shifts to 2.70 eV in DMSO, leading to a bathochromic shift of 0.18 eV.

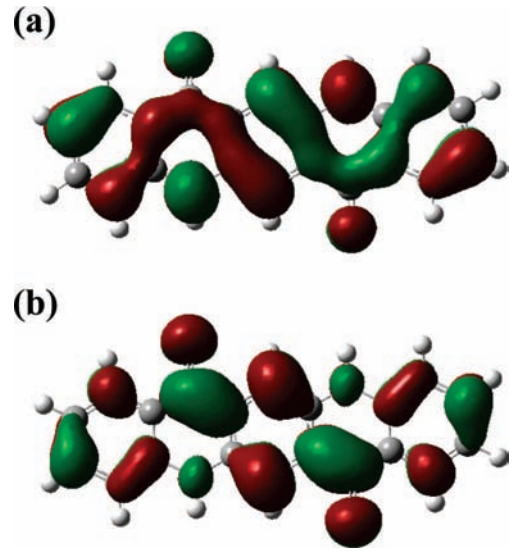

Figure 4. (a) HOMO and (b) LUMO for quinacridone in DMSO solution, obtained with B3LYP/6-31G(d,p)/PCM and the gas-phase RHF optimized geometry.

We also note that in solution the oscillator strength is somewhat enhanced, possibly related to the often observed restriction of the orbital delocalization by the solvent cavity,[49] which leads to the more localized orbitals of the solute. The excitation energy calculated in DMSO is overestimated by 0.33 eV in comparison with the observed value. Some improvement may be obtained by adding a few explicit solvent molecules,[50] since PCM does not take into account solute−solvent charge transfer.

Note that there is a bond length elongation in the solid state (by 0.05−0.17 Å), compared to gas phase. This is thought to be caused largely by the intermolecular hydrogen bonds. There seems to be some correlation between the hydrogen bond energy (Table 2) and the elongated C═O bond length, so that neighbor molecules appear to pull O in C═O. Hydrogen bonding may be influenced to some extent by the crystal field, which is also different in the three phases.

On the basis of TDDFT calculations, the lowest excitation is assigned as the HOMO−LUMO $\pi-\pi^*$ transition. HOMO and LUMO are π orbitals which delocalize over the whole molecule as shown in Figure 4. The direction of the transition dipole points along the short axis of the molecule. We evaluated the Mulliken charges in the ground and excited states (the excited-state electron density was computed and used to obtain the Mulliken charges) and found small differences in N and O atomic charges (0.02e). It suggests that intramolecular charge transfer is very small in the $\pi-\pi^*$ transition of quinacridone.

B. Absorption Spectra in the Crystalline Phases. Table 3 indicates the excitation energies and oscillator strengths obtained with several models. The excitation energies obtained with the 5-mol. models under ESP agree within 0.3 eV with the observed ones. The relative trend in the β-form having a smaller excitation energy than γ is well-reproduced by the best level calculations (that is, 5-mol. with ESP). The value for the α^{I}-form we get is considerably lower than those for the other two forms, which does not agree with experiment (although the absolute value of 2.22 eV is perhaps accidentally exactly reproduced). As is discussed below, the excitation energy shows a clear relation to the C═O bond length and the α^{I} experimental value we used (1.37 Å), which is very different from 1.27 and 1.25 Å for the β- and γ-forms, respectively. The α^{I} experimental structure is quite inaccurate due to difficulties in sample preparation.[51]

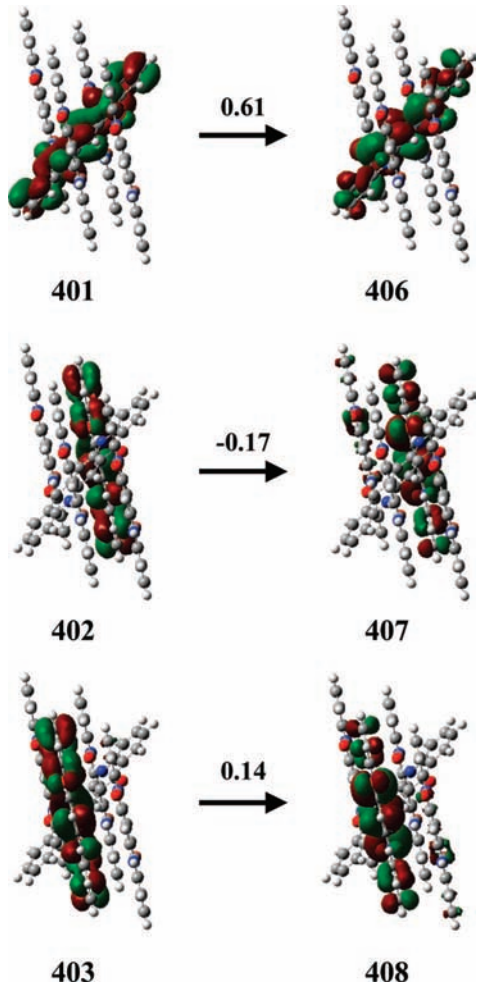

Figure 5. MOs (B3LYP/6-31G(d,p)) participating in the excitation of γ-QA. The numerical values stand for the MO serial number, and the coefficients of this pair in the TDDFT excited-state expansion (whose square gives the weight) are shown above the arrows connecting the occupied MO to the unoccupied MO.

We divide the driving forces influencing the spectral shift into the three factors of the structural deformation, electrostatic potential and intermolecular interactions (other than electrostatic). We define the extent of the spectral shift induced by the structural deformation as the difference between the gas-phase excitation energies obtained with the RHF and the crystal-derived geometries and estimate it to be −0.37, −0.13, and −0.10 eV for the α^{I}-, β-, and γ-phases, respectively. We calculated the effects of electrostatic potential on the spectral shift as −0.14, −0.10, and −0.12 eV for the α^{I}-, β-, and γ-phases, respectively, from the difference between the excitation energies obtained with the 1-mol. model in the gas phase and under ESP. Similar to the ESP influence, we approximate the effect of intermolecular interactions on the spectral shift as the difference between the excitation energies obtained under ESP with the 1- and 5-mol. models and estimate it to be −0.15, −0.18, and −0.17 eV for the α^{I}-, β-, and γ-phases, respectively. Thus, we find that the spectral shift from gas phase to solid phase comes from the cooperation of the structural deformation, electrostatic potential, and intermolecular interactions, and each contribution is of the same order of magnitude.

The oscillator strengths obtained from the 5-mol. models are 2−3 times larger than those with 1-mol. models, suggesting an increase of the electron density participating in the transition. Figure 5 illustrates the occupied and unoccupied molecular orbitals participating in the transition of the γ crystalline phase. Each molecular orbital is almost localized on a single molecule, and there are several coupled excitations appearing as several orbital pairs with a comparable weight. Therefore, the transition can be qualitatively assigned as the superposition of local excitations. This is the reason for larger oscillator strengths in the 5-mol. models. The assignments of the corresponding transitions for the other crystalline phases are similar to that for the γ-phase.

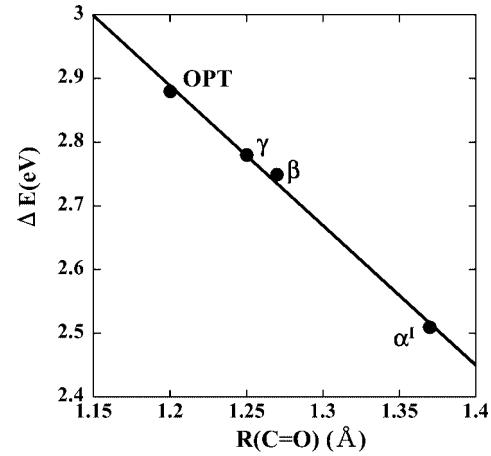

Figure 6. Correlation between the C═O bond length and the TDDFT/B3LYP6-31G(d,p) excitation energy computed for the gas phase (RHF optimized geometry, shown as OPT), and single molecules with the experimental crystal structures for the three phases shown. An auxiliary line is drawn for representing a high correlation (R = 0.997).

C. Dependence of the C═O Bond Length on the Excitation Energy. Because the bond lengths of the C═O group in the crystalline phases become longer than that in the RHF-optimized geometry as shown in Figure 3, we examined the dependence of the C═O bond length on the excitation energy in the linear fashion. As shown in Figure 6, the C═O bond length strongly correlates with the excitation energy; i.e., the longer the C═O bond length, the smaller the excitation energy. Thus, the spectral shift induced by the structural deformation is mainly caused by the stretch of the C═O bond. Furthermore, it should be noted that the small excitation energy in the α^{I}-phase is due to the extraordinary C═O bond length.

D. Contributions from Individual Intermolecular Interactions. To analyze the excitation energy shift induced by individual intermolecular interactions, we carried out FMO-TDDFT calculations which give the individual pair correction terms for the excitation energies showing the explicit quantum effect of the surrounding molecules upon the central one.

Tables 4−6 indicate the two-body correction terms for the α^{I}, β, and γ crystalline phases, respectively, and the indices of the pair counterparts listed in these tables are shown in Figure 7. In the α^{I}-phase, the largest pair contributions come from HB interactions of the 172th with 116th and 228th molecules, and each of them induces a bathochromic shift. The second and the third largest correction terms originate from the non-HB intermolecular interactions and the directions of the energy shift reverse; the former induces a hypsochromic shift by the interactions of the 172th with 123th and 221th molecules, and the latter induces a bathochromic shift by the interactions with the 165th and 179th molecules.

Similarly to the α^{I}-phase, there are three kinds of dominant pair contributions in the β-phase appearing from (a) hydrogen bonding to the 196th with 132th and 260th molecules, (b) the intermolecular interaction with 188th and 204th molecules, and

TABLE 4: Contributions to the Total Excitation Energy in FMO-TDDFT for α^{I}-QA[a]

ID	ΔE_{MI}/eV	δ_{MI}/eV	f
	2.374	0.000	0.077
67	2.370	−0.004	0.149
75	2.380	0.006	0.105
115	2.375	0.001	0.113
116	2.282	−0.092	0.186
123	2.404	0.030	0.106
124	2.375	0.001	0.148
131	2.374	0.000	0.136
164	2.373	−0.001	0.155
165	2.358	−0.016	0.140
171	2.376	0.002	0.150
173	2.376	0.002	0.150
179	2.358	−0.016	0.141
180	2.373	−0.001	0.153
213	2.374	0.000	0.138
220	2.375	0.001	0.149
221	2.404	0.030	0.106
228	2.282	−0.092	0.186
229	2.375	0.001	0.112
269	2.379	0.005	0.106
277	2.370	−0.004	0.149
Total		−0.147	

[a] Pairs are made of the central 172th molecule and one other whose ID is shown.

TABLE 5: Contributions to the Total Excitation Energy in FMO-TDDFT for β-QA[a]

ID	ΔE_{MI}/ eV	δ_{MI}/eV	f
	2.651	0.000	0.069
132	2.546	−0.105	0.151
139	2.650	−0.001	0.087
140	2.635	−0.016	0.120
147	2.650	−0.001	0.076
188	2.685	0.034	0.097
195	2.653	0.002	0.078
197	2.653	0.002	0.077
203	2.651	0.000	0.083
204	2.683	0.032	0.096
205	2.652	0.001	0.074
252	2.635	−0.016	0.117
253	2.650	−0.001	0.079
260	2.542	−0.109	0.075
261	2.650	−0.001	0.072
Total		−0.179	

[a] Pairs are made of the central 196th molecule and one other whose ID is shown.

(c) the intermolecular interaction with 140th and 252th molecules. On the other hand, in the γ-phase, the spectral shift is dominated by the pair contributions coming from HB interactions of the 197th with 196th, 198th, 204th, and 206th molecules and intermolecular interactions with189th and 205th molecules. In this case, HB interactions induce a bathochromic shift, while non-HB intermolecular interactions induce a hypsochromic shift. Thus, the individual intermolecular interactions contribute to bathochromic and hypsochromic shifts depending on the interaction orientation and induce a bathochromic shift overall.

IV. Discussion

We mentioned above that the spectral shift from gas phase to solid phase comes from the cooperation of the structural deformation, electrostatic potential, and intermolecular interactions. As for the structural deformation, the C═O bond is stretched due to the crystal packing, leading to the lowering of the LUMO level while not affecting much the HOMO level. The nature of LUMO can be interpreted as the antibonding π^* orbital for the C═O bond as shown in Figure 4. LUMO is stabilized by the nearly degenerate orbital interaction from individual molecules,[52] leading to the band structure in the infinite limit. Also, the LUMO level is more lowered by the intermolecular interactions than the HOMO level, resulting in a smaller band gap. Thus, all of the driving forces stabilize LUMO cooperatively, and as a result, a bathochromic shift is induced.

TABLE 6: Contributions to the Total Excitation Energy in FMO-TDDFT for γ-QA[a]

ID	ΔE_{MI}/eV	δ_{MI}/eV	f
	2.655	0.000	0.064
125	2.657	0.002	0.121
133	2.655	0.000	0.124
140	2.654	−0.001	0.124
148	2.655	0.000	0.105
188	2.647	−0.008	0.129
189	2.701	0.046	0.084
190	2.646	−0.009	0.118
196	2.577	−0.078	0.124
198	2.579	−0.076	0.125
204	2.575	−0.080	0.121
205	2.701	0.046	0.084
206	2.578	−0.077	0.124
212	2.645	−0.010	0.116
214	2.646	−0.009	0.126
254	2.654	−0.001	0.106
261	2.656	0.001	0.124
262	2.654	−0.001	0.116
269	2.669	0.014	0.075
Total		−0.241	

[a] Pairs are made of the central 197th molecule and one other whose ID is shown.

The relative excitation energies for all crystalline phases we obtained with TDDFT seem to be in a reasonable agreement with experiment, excluding the α^{I}-phase, where the experimental structure we used has an unusually long C═O bond. The FMO-TDDFT calculations are based on pairs corrections, and thus have a somewhat limited accuracy in this regard; however, they are conducted for large conglomerates (14−20 molecules). We consider these calculations useful especially for the relative comparison of pair contributions in the three forms, and discerning the orientation impact upon the excitation energy.

Figure 8 shows the dependence of the number of molecules on the excitation energy obtained with the one-dimensional hydrogen bonding chain of α^{I}-QA. The excitation energy abruptly decreases at dimer and converges around pentamer. In pentamer, the molecular orbitals participating in the excitation distribute over the whole molecular system. This indicates that hydrogen bonding interactions influence the excitation energy over a wide range, suggesting the use of a large cluster model for more accurate calculations. It is noted in passing that the size dependence of the band gap upon the linear size d in nanostructures is known as the quantum confinement effect,[53] which has the $A + Cd^{-k}$ form, where A, C, and k are constants. In this case, the parameters are as follows; $A = 2.22$, $C = 0.30$, and $k = 2.17$. Our linear cluster of QA molecules also appears to display a similar dependence, since the excitation energy in Figure 8 is related to the band gap (HOMO−LUMO gap).

Figure 8 clearly shows the importance of the many-body effects. The two-body term contributes about 0.25 eV, and this bulk contribution for all pairs can be reliably obtained with FMO-TDDFT. Higher body terms contribute about 0.05 eV

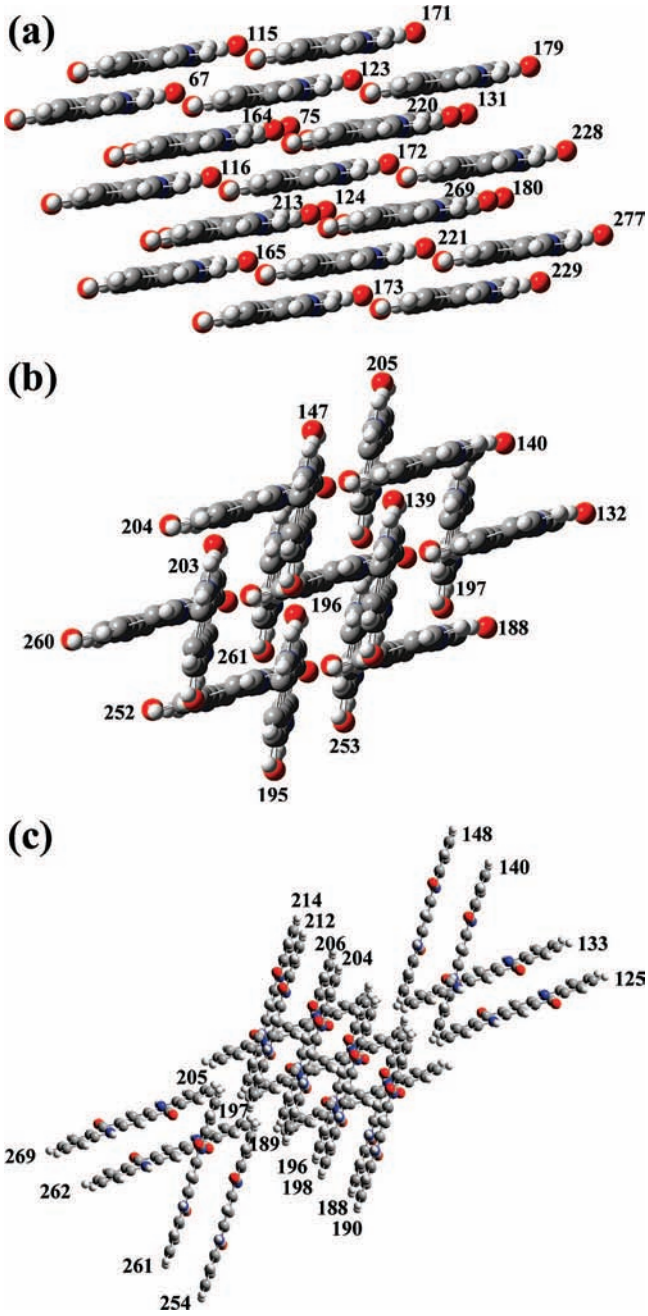

Figure 7. Central part of the larger cluster used in FMO-TDDFT for the (a) α^{I}-, (b) β-, and (c) γ-phases. The numbers shown are for the molecular IDs listed in Tables 4−6.

more. This suggests that subtle energy difference on the order of 0.05 eV may not be well-reproduced by FMO-TDDFT for the large clusters involving degenerate states.

In general, there are two approaches for such systems. One is a direct calculation of crystal under the periodic boundary conditions, and the other is an approximate large cluster calculation, e.g., with FMO-TDDFT. Molecules in crystal generally make the band structure which determines the optical properties. Therefore, the best solution is the excited-state calculation based on DFT with the periodic boundary conditions; however, such methods have not been developed, to the best of our knowledge.

On the other hand, the FMO-TDDFT method is best suited for molecular clusters which do not exhibit total orbital delocalization and the degenerate states. Table 7 gives comparison between the excitation energies obtained with FMO-TDDFT calculations and the corresponding TDDFT ones. For the former, we extracted the same four pair contributions, corresponding to the 5-mol. model of TDDFT. In addition, full FMO-TDDFT values made of 14−20 contributions are also listed, showing the importance of the longer range corrections.

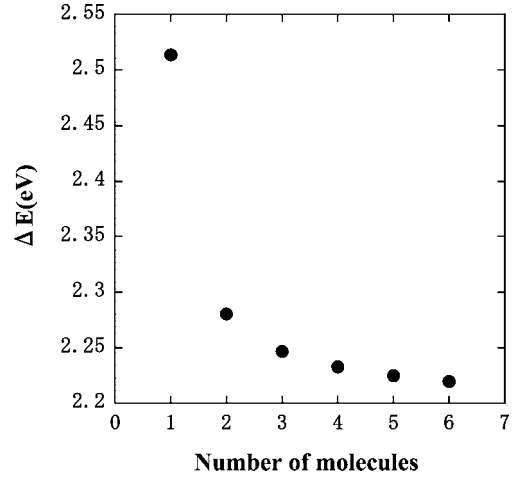

Figure 8. Dependence of the TDDFT/B3LYP/6-31G(d,p) excitation energy in the one-dimensional hydrogen-bonded chain of α^{I}-QA upon the cluster size.

TABLE 7: Comparison between TDDFT and FMO-TDDFT Results (ΔE, eV)

		TDDFT		FMOΔE	
model	IDs	ΔE	f	partial[a]	total[b]
α^{I}					
3-mol. HB	172, 116, 228	2.25	0.19	2.19	
3-mol. non-HB	172, 123, 221	2.42	0.12	2.43	
5-mol.	172, 116, 228, 123, 221	2.22	0.17	2.25	2.23
β					
3-mol. HB	196, 132, 260	2.51	0.26	2.44	
3-mol. non-HB	196, 188, 204	2.69	0.03	2.72	
5-mol.	196, 132, 260, 188, 204	2.47	0.16	2.50	2.47
γ					
3-mol. HB	197, 196, 198	2.55	0.23	2.50	
3-mol. HB	197, 196, 206	2.56	0.26	2.50	
3-mol. HB	197, 198, 204	2.54	0.18	2.50	
5-mol.	197, 196, 198, 204, 206	2.49	0.22	2.34	2.41

[a] Including only four pair corrections (corresponding to the 5-mol. model). [b] Including all (14−20) pair corrections.

The excitation energies obtained with FMO-TDDFT for 3-mol. HB models are underestimated, while the excitation energies for 3-mol. non-HB models are overestimated. The errors for the 5-mol. models including HB and non-HB interactions are estimated at 0.03, 0.03, and −0.15 eV for the α^{I}-, β-, and γ-phases, respectively. Small errors in the α^{I}- and β-phases may be due to accidental cancelation of plus and minus contributions, while in the γ-phase larger error is obtained because of unbalanced cancelation. Thus, the accuracy for the aggregation systems strongly depends on the interaction manner. The occurrence of the errors is due to the many-body interactions, and it would be desirable to improve the FMO-TDDFT method including higher many-body effects, e.g., by including triple corrections.[30]

V. Conclusions

On the basis of the TDDFT calculations, we determined that the spectral shift from gas phase to the solid state in QA is dominated by the cooperation of the structural deformation, the electrostatic potential and the intermolecular interactions. We

also computed the values for all three contributions, which are of the same order of magnitude. The spectral shift induced by the structural deformation is mainly caused by the stretch of the C═O bond. The individual intermolecular interactions contribute to bathochromic and hypsochromic shifts, depending on the interaction manner, and induce a bathochromic shift overall.

Thus, in the present study we can clarify the orientation factor upon the excitation energy lowering, which can provide clues for the pigment design. In addition, we suggest that for a better prediction of the excitation energies in the crystalline phases of the pigments, it would be required to develop a novel theoretical framework including the improvement of FMO-TDDFT, in which the many-body effects of orbital delocalization over a wide range are taken into account. Some improvement can be obtained with a better functional, which describes the dispersion and is more reliable for charge-transfer effects.

Acknowledgment. This work was supported in part by the Next Generation Super Computing Project, Nanoscience Program (MEXT, Japan), and from a Grant-in-Aid for Scientific Research (JSPS, Japan).

References and Notes

(1) Potts, G. D.; Jones, W.; Bullock, J. F.; Andrews, S. J.; Maginn, S. J. *J. Chem. Soc., Chem. Commun.* **1994**, 2565.
(2) Lincke, G.; Finzel, H.-U. *Cryst. Res. Technol.* **1996**, *31*, 441.
(3) Mizuguchi, J.; Sasaki, T.; Tojo, K. *Z. Kristallogr.* **2002**, *217*, 249.
(4) Nishimura, N.; Senju, T.; Mizuguchi, J. *Acta Crystallogr.* **2006**, *E62*, o4683.
(5) Paulus, E. F.; Leusen, F. J. J.; Schmidt, M. U. *CrystEngComm* **2007**, *9*, 131.
(6) Panina, N.; Leusen, F. J. J.; Jansen, F. F. B. J.; Verwer, P.; Meekes, H.; Vlieg, E.; Deroover, G. *J. Appl. Crystallogr.* **2007**, *40*, 105.
(7) Yokoyama, Y. *Bull. Chem. Soc. Jpn.* **1983**, *56*, 1775.
(8) Minami, N.; Yokoyama, Y. *Kenkyu Hokoku-Sen'i Kobunshi Zairyo Kenkyusho* **1992**, *171*, 7.
(9) Filho, D. S.; Oliveira, C. M. F. *J. Mater. Sci.* **1992**, *27*, 5101.
(10) Sugiyama, T.; Asahi, T.; Takeuchi, H.; Masuhara, H. *Jpn. J. Appl. Phys.* **2006**, *45*, 384.
(11) Mizuguchi, J.; Endo, A.; Matsumoto, S. *J. Imag. Soc. Jpn. (Nippon Gazo Gakkaishi)* **2000**, *39*, 94.
(12) Ni, J. P.; Chen, J.; Ueda, Y. *Mol. Cryst. Liq. Cryst.* **2001**, *370*, 257.
(13) Mizuguchi, J.; Senju, T. *IS&T's NIP19: Int. Conf. Digital Print. Technol.* **2003**, 678.
(14) Mizuguchi, J.; Senju, T. *J. Phys. Chem. B* **2006**, *110*, 19154.
(15) Senju, T.; Mizuguchi, J. *Dyes Pigments* **2008**, *76*, 760.
(16) Yatsenko, A. V. *J. Mol. Model.* **2003**, *9*, 207.
(17) Susanto, A.; Mozo, R.; Muhida, R.; Kishi, T.; Rahman, M. M.; Dino, W. A.; Dipojono, H. K.; Kasai, H *Eur. Phys. J. D* **2006**, *38*, 199.
(18) Mizuguchi, J. *J. Phys. Chem. A* **2000**, *104*, 1817.
(19) Mizuguchi, J.; Tojo, K. *J. Phys. Chem. B* **2002**, *106*, 767.
(20) Runge, E.; Gross, E. K. U. *Phys. Rev. Lett.* **1984**, *52*, 997.
(21) Bauernschmitt, R.; Ahlrichs, R. *Chem. Phys. Lett.* **1996**, *256*, 454.
(22) Stratmann, R. E.; Scuseria, G. E. *J. Chem. Phys.* **1998**, *109*, 8218.
(23) Van Gisbergen, S. J. A.; Guerra, C. F.; Baerends, E. J. *J. Comput. Chem.* **2000**, *21*, 1511.
(24) Furche, F.; Ahlrichs, R. *J. Chem. Phys.* **2002**, *117*, 7433. Erratum: Furche, F.; Ahlrichs, R. *J. Chem. Phys.* **2004**, *121*, 12772.
(25) Autschbach, J.; Ziegler, T. *J. Chem. Phys.* **2002**, *116*, 891.
(26) Nakatsuji, H. *Chem. Phys. Lett.* **1978**, *59*, 362.
(27) Nakatsuji, H.; Hirao, K. *J. Chem. Phys.* **1978**, *68*, 2053.
(28) Kitaura, K.; Ikeo, E.; Asada, T.; Nakano, T.; Uebayasi, M. *Chem. Phys. Lett.* **1999**, *313*, 701.
(29) Nakano, T.; Kaminuma, T.; Sato, T.; Akiyama, Y.; Uebayasi, M.; Kitaura, K. *Chem. Phys. Lett.* **2000**, *318*, 614.
(30) Fedorov, D. G.; Kitaura, K. *J. Chem. Phys.* **2004**, *120*, 6832.
(31) Sugiki, S.; Kurita, N.; Sengoku, Y.; Sekino, H. *Chem. Phys. Lett.* **2003**, *382*, 611.
(32) Fedorov, D. G.; Kitaura, K. *J. Chem. Phys.* **2004**, *121*, 2483.
(33) Fedorov, D. G.; Kitaura, K. *J. Chem. Phys.* **2005**, *122*, 054108.
(34) Fedorov, D. G.; Kitaura, K. *J. Chem. Phys.* **2005**, *123*, 134103.
(35) Mochizuki, Y.; Koikegami, S.; Amari, S.; Segawa, K.; Kitaura, K.; Nakano, T. *Chem. Phys. Lett.* **2005**, *406*, 283.
(36) Mochizuki, Y.; Tanaka, K.; Yamashita, K.; Ishikawa, T.; Nakano, T.; Amari, S.; Segawa, K.; Murase, T.; Tokiwa, H.; Sakurai, M. *Theor. Chem. Acc.* **2007**, *117*, 541.
(37) Chiba, M.; Fedorov, D. G.; Kitaura, K. *Chem. Phys. Lett.* **2007**, *444*, 346.
(38) Chiba, M.; Fedorov, D. G.; Kitaura, K. *J. Chem. Phys.* **2007**, *127*, 104108.
(39) Fedorov, D. G.; Kitaura, K. In *Modern Methods for Theoretical Physical Chemistry of Biopolymers*; Starikov, E. B., Lewis, J. P., Tanaka, S., Eds.; Elsevier: Amsterdam, 2006; pp 3−38.
(40) Fedorov, D. G.; Kitaura, K. *J. Phys. Chem. A* **2007**, *111*, 6904.
(41) Hariharan, P. C.; Pople, J. A. *Theor. Chim. Acta* **1973**, *28*, 213.
(42) Becke, A. D. *Phys. Rev. A* **1988**, *38*, 3098.
(43) Lee, C.; Yang, W.; Parr, R. G. *Phys. Rev. B* **1988**, *37*, 785.
(44) Becke, A. D. *J. Chem. Phys.* **1993**, *98*, 5648.
(45) Miertus, S.; Scrocco, E.; Tomasi, J. *Chem. Phys.* **1981**, *55*, 117.
(46) Miertus, S.; Tomasi, J. *Chem. Phys.* **1982**, *65*, 239.
(47) Frisch, M. J.; Trucks, G. W.; Schlegel, H. B.; Scuseria, G. E.; Robb, M. A.; Cheeseman, J. R.; Montgomery, J. A., Jr.; Vreven, T.; Kudin, K. N.; Burant, J. C.; Millam, J. M.; Iyengar, S. S.; Tomasi, J.; Barone, V.; Mennucci, B.; Cossi, M.; Scalmani, G.; Rega, N.; Petersson, G. A.; Nakatsuji, H.; Hada, M.; Ehara, M.; Toyota, K.; Fukuda, R.; Hasegawa, J.; Ishida, M.; Nakajima, T.; Honda, Y.; Kitao, O.; Nakai, H.; Klene, M.; Li, X.; Knox, J. E.; Hratchian, H. P.; Cross, J. B.; Bakken, V.; Adamo, C.; Jaramillo, J.; Gomperts, R.; Stratmann, R. E.; Yazyev, O.; Austin, A. J.; Cammi, R.; Pomelli, C.; Ochterski, J. W.; Ayala, P. Y.; Morokuma, K.; Voth, G. A.; Salvador, P.; Dannenberg, J. J.; Zakrzewski, V. G.; Dapprich, S.; Daniels, A. D.; Strain, M. C.; Farkas, O.; Malick, D. K.; Rabuck, A. D.; Raghavachari, K.; Foresman, J. B.; Ortiz, J. V.; Cui, Q.; Baboul, A. G.; Clifford, S.; Cioslowski, J.; Stefanov, B. B.; Liu, G.; Liashenko, A.; Piskorz, P.; Komaromi, I.; Martin, R. L.; Fox, D. J.; Keith, T.; Al-Laham, M. A.; Peng, C. Y.; Nanayakkara, A.; Challacombe, M.; Gill, P. M. W.; Johnson, B.; Chen, W.; Wong, M. W.; Gonzalez, C.; Pople, J. A. Gaussian: Wallingford, CT, 2004.
(48) Schmidt, M. W.; Baldridge, K. K.; Boatz, J. A.; Elbert, S. T.; Gordon, M. S.; Jensen, J. H.; Koseki, S.; Matsunaga, N.; Nguyen, K. A.; Su, S. J.; Windus, T. L.; Dupuis, M.; Montgomery, J. A. *J. Comput. Chem.* **1993**, *14*, 1347.
(49) Chiba, M.; Fedorov, D. G.; Kitaura, K. *J. Comput. Chem.*, in press.
(50) Cossi, M.; Barone, V. *J. Chem. Phys.* **2001**, *115*, 4708.
(51) Schmidt, M. U. Private communication.
(52) Avramov, P. V., Fedorov, D. G., Sorokin, P. B., Chernozatonskii, L. A., Ovchinnikov, S. G. *J. Appl. Phys.* **2008**, *104*, 054305.
(53) Avramov, P. V.; Fedorov, D. G.; Sorokin, P. B.; Chernozatonskii, L. A.; Gordon, M. S. *J. Phys. Chem. C* **2007**, *111*, 18824.

JP804943M